ACS OMEGA

http://pubs.acs.org/journal/acsodf

Article

Investigating the Flexural Behavior of a Two-Span High-Performance Concrete Beam Using Experimentally Derived Stress Block Parameters

Asif Iqbal A. Momin,* Aijaz Ahmad Zende,* Rajesab B. Khadiranaikar, Abdullah H. Alsabhan, Shamshad Alam, Mohammad Amir Khan, and Mohammad Obaid Qamar

Cite This: *ACS Omega* 2023, 8, 17992−17999

Read Online

ACCESS | Metrics & More | Article Recommendations

ABSTRACT: High-performance concrete (HPC) is increasingly used in construction due to its superior strength and durability. However, current stress block parameters used for designing normal-strength concrete cannot be safely applied to HPC. To address this issue, new stress block parameters have been proposed through experimental works, which are used for designing HPC members. In this study, the behavior of HPC was investigated using these stress block parameters. Two-span beams made of HPC were tested under five-point bending, and an idealized stress block curve was derived from the experimental stress−strain curve for grades 60, 80, and 100 MPa. Based on the stress block curve, equations for the ultimate moment of resistance, depth of the neutral axis, limiting moment of resistance, and maximum depth of the neutral axis were proposed. An idealized load−deformation curve was also developed, which identified four significant events: first cracking, yielding of reinforced steel, crushing of concrete with spalling of cover, and ultimate failure. The predicted values were found to be in good agreement with the experimental values, and the average location of the first crack was identified to be 0.270 L, measured from the central support on either side of the span. These findings provide important insights for the design of HPC structures, contributing to the development of more resilient and durable infrastructure.

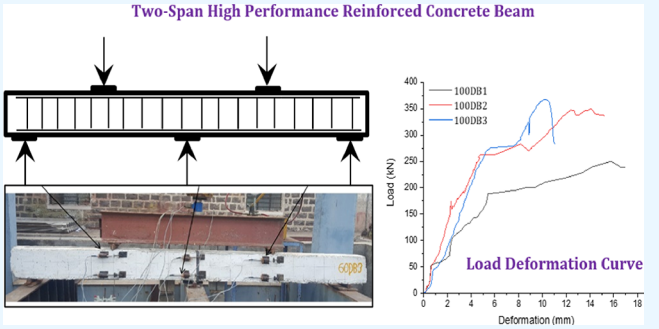

1. INTRODUCTION

Concrete is the most commonly utilized building material across the world. It has been used for centuries in the construction of various types of structures, from simple residential buildings to complex bridges and high-rise buildings. In the past few years, the demand for high-performance concrete (HPC) has increased due to its superior properties and improved performance compared to conventional concrete. HPC is a type of concrete that has enhanced mechanical, physical, and chemical properties that are achieved by using a combination of advanced admixtures and/or high-strength cementitious materials. Innovations in concrete technology have led to the development of high-strength concretes such as high-strength concrete (HSC) and high-performance concrete (HPC), which have increased compressive strength and better long-term performance than conventional concrete.[1,2] HPC offers several advantages over conventional concrete, including lower permeability, enhanced durability, and greater resistance to environmental factors.[3,4] Reinforced HPC exhibits superior flexural behavior compared to reinforced normal strength concrete (NSC) or HSC, underscoring the importance of investigating its behavior under flexure. The design of reinforced concrete beams is governed by the strength and deformation characteristics of concrete under different types of loads, including flexure, shear, and axial loads. The study of the flexural behavior of reinforced concrete beams is of paramount importance to design a safe and reliable structure.

Designing HPC beams to withstand flexure can be a challenging task, as most standard codes and methods used for NSC cannot be applied to HSC.[5,6] To study the flexural behavior of higher-strength concretes, researchers have put forward stress block parameters and verified their experimental results, proposing substantial changes to current codes.[7−14] Stress block parameters have also been proposed for special types of concretes, such as geopolymer concrete (GPC).[15,16] However, it is unclear whether these parameters can be applied

Received: February 22, 2023
Accepted: April 25, 2023
Published: May 9, 2023

to HPC. While the ultimate strain of concrete recommended by the American code 441-R96[17] is 0.003, other codes such as EC-2,[18] Canadian code,[19] and IS Code[20] limit it to 0.0035. Therefore, it is necessary to conduct a thorough investigation of the design recommendations provided by various codes to accurately determine the strength of HPC beams under flexure.

This research aims to investigate the flexural behavior of two-span HPC beams with the help of experimental investigation and numerical analysis. The stress block parameters proposed for HSC and GPC will be examined for their applicability to HPC beams. The study will include the effect of various parameters, like beam depth, reinforcement ratio, and span-to-depth ratio, on the flexural behavior of HPC beams. This study will also provide insight into the behavior of HPC beams under flexure, and the results will be compared with the predictions of different codes. The knowledge gained from this study will be useful in designing safe and economical HPC beams under flexure, which will ultimately result in the development of safer and more durable structures.

The introductory section presents a brief overview of the importance of HPC in construction and the challenges associated with designing HPC members using current stress block parameters developed for normal-strength concrete. The study proposes new stress block parameters through experimental investigation and uses them to investigate the behavior of HPC. The testing procedure, including the preparation of the specimens, instrumentation, and loading arrangement, is described, followed by a detailed explanation of the data analysis methods, including the derivation of the idealized stress block curve and equations for the ultimate moment of resistance, depth of the neutral axis, limiting moment of resistance, and maximum depth of the neutral axis. Finally, the development of the load−deformation curve and the identification of the four significant events are explained. The paper aims to enhance the clarity and organization and emphasizes the significance of the findings for the design of HPC structures.

2. METHODOLOGY

The current study aims to explore the performance of reinforced HPC beams in a five-point bending test, conducted experimentally on two-span beams, as illustrated in Figure 1.

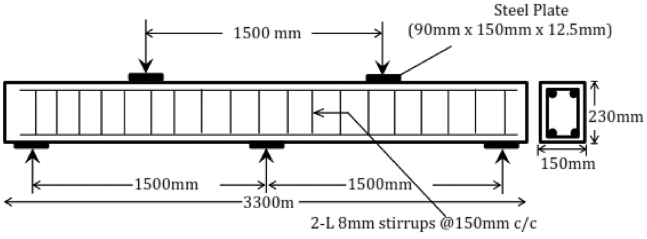

Figure 1. Two-span continuous HPC beam specimen in flexure.

Eight beams, as presented in Table 1, were cast for the flexure test and subjected to a monotonic single-point load at each span under five-point bending. The concrete grade and the longitudinal tension reinforcement were varied in this experimental program. The rectangular beam size of 150 mm × 230 mm with a span length of 1500 mm is chosen for the test specimens for the flexure test. The HPC beams for the above-stated strength were cast for different areas of tension and compression steel to investigate the behavior of under-reinforced sections. For the casting of the beam specimen, steel of grade Fe-500 was used throughout the investigation in the current study. To prevent shear failure according to IS-code specifications, two-legged transverse reinforcements with a diameter of 10 mm were provided at a spacing of 100 mm. To ensure even distribution of stress, steel plates measuring 90 mm by 150 mm by 12.5 mm are placed at the beam's supports and loading points. Compressive and tensile strains are measured using LVDTs affixed at the midpoint and center support of the specimens along the beam's depth. To measure deformations of the hinge portion, a series of four LVDTs were fixed at the expected position of the plastic hinges. The position of these LVDTs is shown in Figure 2. A bearing of 150 mm on either side was provided to provide an overall length of 3.3 m. To ensure adequate stiffness at the mid-support of each beam, a pair of plates measuring 150 mm by 150 mm is incorporated into the beam, as demonstrated in Figure 3.

3. STRESS BLOCK PARAMETERS

Various codal provisions have unique stress block parameters, which usually apply to a compressive strength lower than 50 MPa. As a result, efforts are being made to establish stress block parameters specifically for high-performance concrete (HPC). An idealized stress block curve for HPC is derived based on experimental data that takes into account three different concrete strength ranges. Polynomial curves that best fit the observed behavior of each concrete grade were drawn using data from experiments and a literature review.[21−26] These curves are presented in Figure 4. An idealized stress block curve, illustrated in Figure 5, is obtained by using the curves derived from the polynomial fitting of the experimental and literature survey data. The coefficients k_1, k_2, and k_3 represent the stress factor, centroid factor, and area factor, respectively. The value of k_1 is obtained by taking the mean of the stress values at ultimate strain, which is confirmed by other researchers.[27] The approximation of the k_1 value was found to be consistent with the literature review. Additionally, for k_2 and k_3, which are obtained from an assumed stress block, the approximated values were found to be comparable to those reported in the literature. The values of x_1 and x_2 can be determined from the strain diagram as follows:

$$x_1 = \frac{2}{3}x_u \text{ and } x_2 = \frac{1}{3}x_u \quad (1)$$

The stress factor k_1 is computed as the average stress at ultimate strain from experimental results for three concrete grades. The area factor k_3 was determined by calculating the area of the stress blocks. Values of k_1 and k_3 are found to be 0.896 and 0.777, respectively.

Equation 2 provides a method to determine the depth of the centroid of compression zone from the extreme compression fiber by taking the moment of area. Using this method, the centroid factor k_2 was found to be 0.405.

$$\bar{x} = 0.405x_u \quad (2)$$

The total compressive force can be calculated using eq 3, which takes into account the coefficients k_1, k_2, and k_3 and a partial safety factor of 1.3.

$$C_u = 0.535f_{ck}bx_u \quad (3)$$

The flexural strength of an HPC beam section can be determined by taking the moment of the compressive force, C_u or T_u, using eqs 4 and 5, which is based on the stress block parameters discussed above. Equations 6 and 7 give the depth of neutral axis (NA) and limiting moment of resistance.

https://doi.org/10.1021/acsomega.3c01197
ACS Omega 2023, 8, 17992−17999

Table 1. Details of Beam Specimens

			longitudinal reinforcement		% of reinforcement (ρ)			longitudinal reinforcement ratio ρ/ρ_b	
designation	target concrete strength (MPa)	cube strength (MPa), f_{ck}	tension	compression	tension	compression	balanced reinforcement, ρ_b	tension	compression
60DB1	60	84.98	3 # 12 mm	2 # 16 mm	1.209	1.433	4.823	0.251	0.297
60DB2		85.85	2 # 16 + 1 # 10 mm	3 # 16 mm	1.713	2.150	4.873	0.352	0.441
60DB3		83.64	3 # 16 mm	2 # 20 + 1 # 12 mm	2.173	2.671	4.747	0.458	0.563
80DB1	80	90.21	3 # 10 mm	2 # 12 + 1 # 8 mm	0.831	0.975	5.120	0.162	0.190
80DB2		87.79	2 # 12 + 1 # 8 mm	2 # 16 mm	0.975	1.418	4.983	0.196	0.285
100DB1	100	107.68	3 # 12 mm	2 # 16 mm	1.197	1.418	6.112	0.196	0.232
100DB2		108.61	2 # 16 + 1 # 10 mm	3 # 16 mm	1.713	2.150	6.165	0.278	0.349
100DB3		102.73	3 # 16 mm	2 # 20 + 1 # 12 mm	2.173	2.671	5.831	0.373	0.458

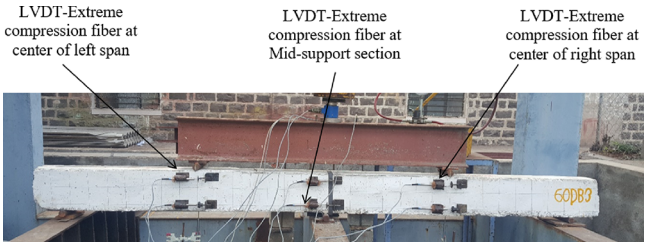

Figure 2. Beam specimen with LVDTs to measure ultimate strain. Photograph courtesy of Aijaz Ahmad Zende. Copyright 2023.

$$M_u = 0.535 f_{ck} b x_u (d - 0.405 x_u) \quad (4)$$

$$M_u = 0.87 f_y A_{st} d \left(1 - 0.658 \frac{A_{st} f_y}{f_{ck} b d}\right) \quad (5)$$

Table 2 presents the proposed equations and stress block parameters.

4. FLEXURAL BEHAVIOR OF TWO-SPAN HPC BEAMS

In the case of two-span HPC beams, the ultimate moment of failure by experiment is calculated using the moment-distribution method. The maximum positive moment is considered the failure moment under ultimate load. The equations for maximum positive and negative moments as derived by the moment-distribution method are given by eqs 8 and 9.

The ultimate moment of resistance is predicted using the defined stress block parameters. The stress block-derived ultimate moment of resistance ranges between 0.81 and 1.02 times the experimental ultimate moment at failure, as shown in

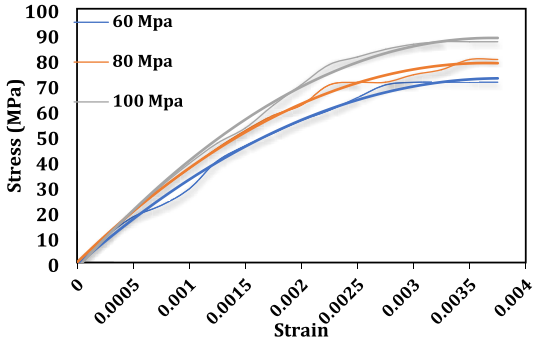

Figure 4. Stress−strain curves for HPC.

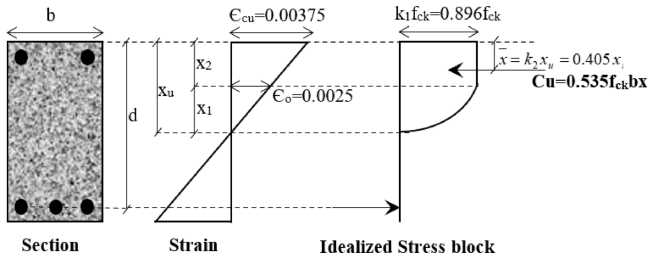

Figure 5. Equivalent stress block parameters.

the results presented in Figure 6 and Table 3. The graph depicts a variation in the ratio of the predicted ultimate moment to the experimental moment as a function of tension reinforcement percentage and concrete characteristic strength. Figure 7 also depicts the variation of the ratios M_u/bd^2 for both the predicted and experimental moments of resistance for the M_{60} grade of HPC. Hence, it can be noted that the above equation for the

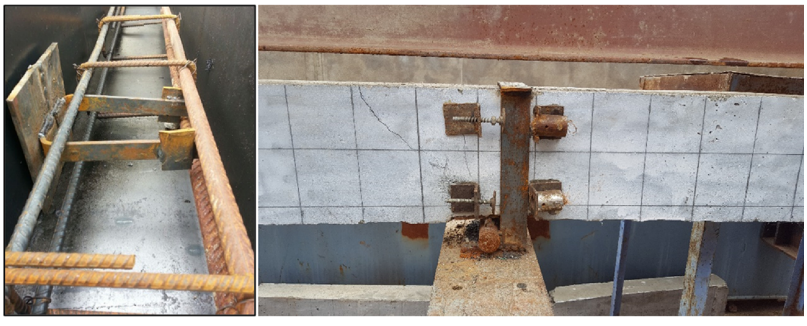

Figure 3. Connection at mid-support. Photograph courtesy of Aijaz Ahmad Zende. Copyright 2023.

https://doi.org/10.1021/acsomega.3c01197
ACS Omega 2023, 8, 17992−17999

Table 2. Stress Block Parameters and Proposed Equations

parameter	equation/value
stress factor k_1	$k_1 = 0.896$
centroid factor k_2	$k_2 = 0.405$
area factor k_3	$k_3 = 0.777$
flexural strength of reinforced HPC beam	$M_u = 0.535 f_{ck} b x_u (d - 0.405 x_u)$, $M_u = 0.87 f_y A_{st} d\left(1 - 0.658 \frac{A_{st} f_y}{f_{ck} bd}\right)$
depth of NA	$x_u = \frac{0.87 f_y A_{st}}{0.535 f_{ck} b}$ (6)
limiting moment of resistance	$M_{ulim} = 0.1934 f_{ck} bd^2$ (7)

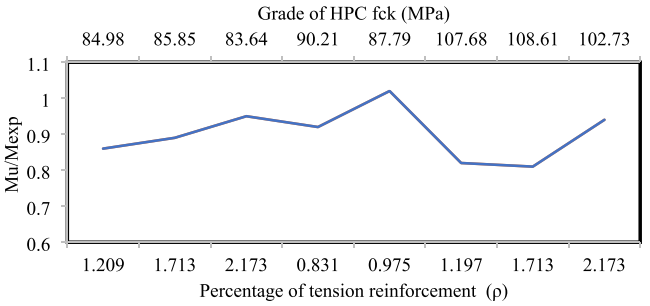

Figure 6. Variation of M_u/M_{exp} with ρ and grade of concrete.

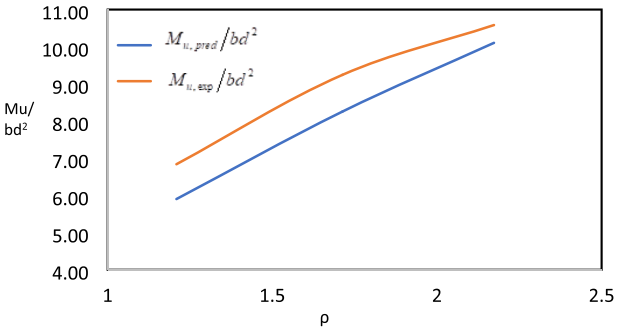

Figure 7. Variation of M_u/bd^2 with ρ for M_{60} grade.

moment of resistance predicts desirable results for continuous beams.

$$M_{u,+ve} = 0.15625wL \quad (8)$$

$$M_{u,-ve} = 0.1875wL \quad (9)$$

4.1. Load−Deflection Variation. The experimental data in Figures 8−10 depict load versus deflection curves of two-span HPC beam specimens. During the testing process, it was seen that the deformation capacities of some HPC beams decrease as the tension steel reinforcement increases at nearly the same load levels. This suggests that ductility increases by decreasing the tension steel reinforcement since the longitudinal steel reinforcement ratio has a greater impact than the strength of the concrete. Figure 11 displays an idealized load−deformation curve based on all beam specimens. The curve is divided into four segments, labeled A, B, C, and D, representing significant events observed during the experiments: first cracking, yielding of reinforced steel, crushing of concrete with spalling of cover, and ultimate failure, respectively. This idealized curve represents the behavior of all HPC beams tested in the study. The load−deformation curve in zones A and B corresponds to reduced beam stiffness, while zones C and D represent a reduction in the applied load. This behavior was observed in all tested beams.

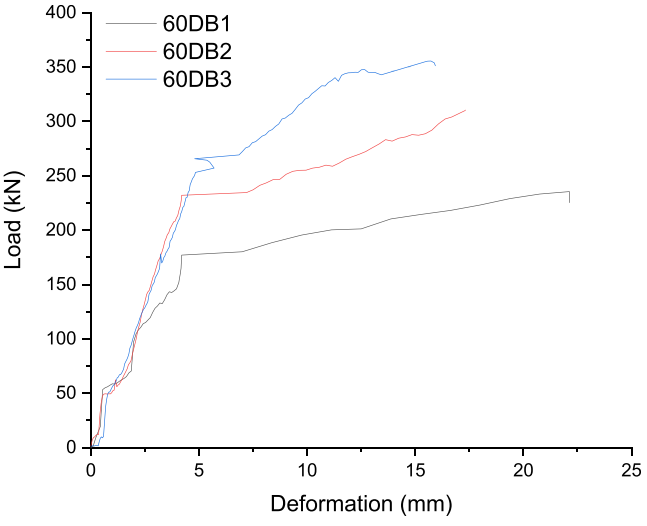

Figure 8. Load−deflection curve for M_{60} grade.

The selected experimental beam models were designed to be under-reinforced and were confirmed to be so after testing. The

Table 3. Flexural Experimental Test Results

designation	d	f_{ck} (MPa)	ρ (%)	P_u (kN)	x_u (mm)	$M_{u,exp}$ (kN m)	$M_{u,pred}$ (kN m)	$M_{u,pred}/M_{u,exp}$
60DB1	164	84.98	1.209	235.45	22.55	27.59	23.81	0.86
60DB2	162	85.85	1.713	310.50	31.62	36.39	32.50	0.89
60DB3	162	83.64	2.173	355.50	40.73	41.66	39.77	0.95
80DB1	237	90.21	0.831	228.00	14.75	26.72	24.67	0.92
80DB2	236	87.79	0.975	240.00	17.78	28.13	28.67	1.02
100DB1	164	107.68	1.197	250.00	17.79	29.30	24.11	0.82
100DB2	162	108.61	1.713	349.60	24.99	40.97	33.08	0.81
100DB3	162	102.73	2.173	367.50	33.16	43.07	40.61	0.94

https://doi.org/10.1021/acsomega.3c01197
ACS Omega 2023, 8, 17992−17999

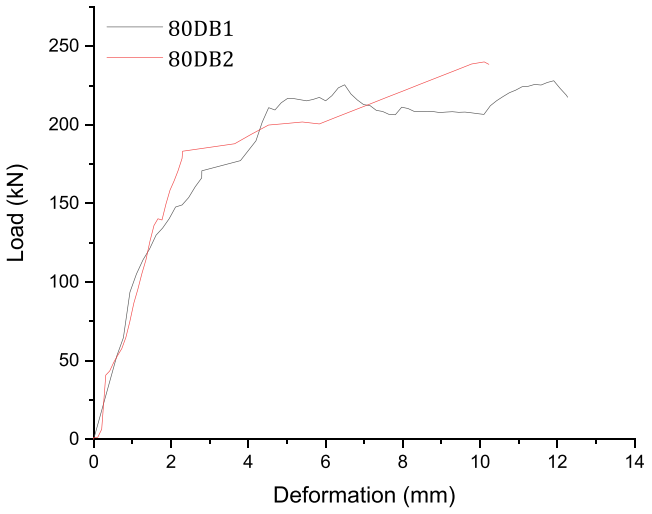

Figure 9. Load−deflection curve for M_{80} grade.

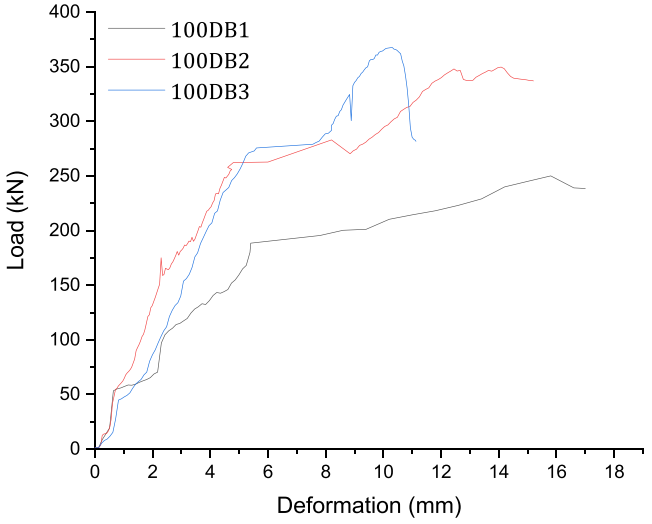

Figure 10. Load−deflection curves for M_{100} grade.

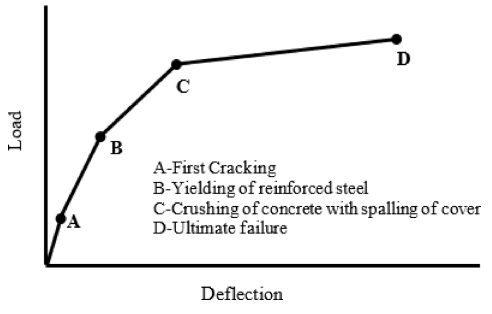

Figure 11. Ideal load−deflection curve.

results of the experiments, including load, deflection, and the location of the first visible crack, are shown in Table 4. The first visible cracks were measured from the observer's left support, and the deflections at failure were also recorded. As shown in Figure 12, the load at the first visible crack increased as the percentage of longitudinal tension steel and the grade of HPC increased. The average location of the first crack was found to be 0.270 L, measured from the central support on either side of the span. The beams failed in the tension zone, with a mean load of 76.70% of the ultimate load. The load at the first visible crack

Table 4. Observations at First Crack for Two-Span HPC Beam Specimens

beam designation	percentage of longitudinal tension steel (%)	load at first crack (kN)	deflection at first crack (mm)	location of first crack from the left support of the observer in the tension zone (mm)	crack width at failure (mm)
60DB1	1.209	180	7.00	0.61 L	2.5
60DB2	1.713	222	6.80	0.30 L	2.5
60DB3	2.173	248	7.60	0.09 L	2.3
80DB1	0.831	182	4.00	0.17 L	2.2
80DB2	0.975	187	3.65	0.21 L	2.1
100DB1	1.197	193	7.80	0.17 L	1.8
100DB2	1.713	263	8.52	0.30 L	1.7
100DB3	2.173	294	8.10	0.31 L	1.7

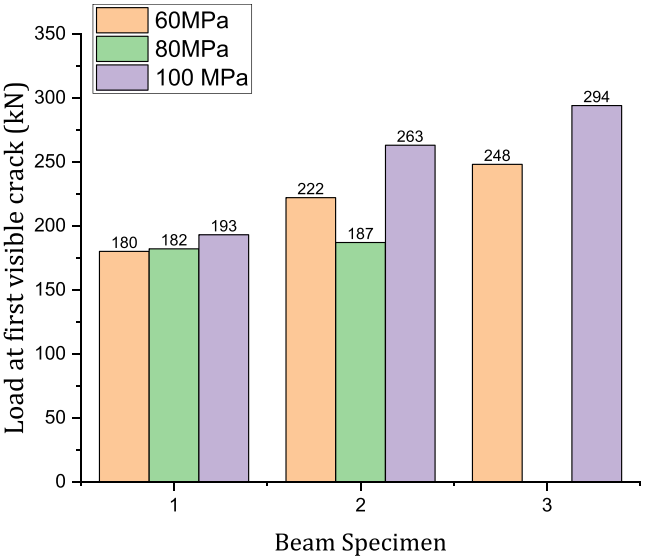

Figure 12. Load at first visible crack for two-span HPC beam specimens.

increased with an increase in the longitudinal reinforcement ratio. As the load increased, the cracks propagated due to the yielding of the reinforcing steel, followed by crushing of the concrete and spalling of the cover at the compression zones. Last, the load-carrying capacity was lost with the formation of a greater number of cracks. These results are important as they provide valuable information on the behavior of under-reinforced HPC beams under loading.

4.2. Crack Propagation. Figures 13−15 show the crack patterns and failure modes of beams tested for all grades. When the load was applied to the test specimen, a few hair cracks were seen, and with the further increase in load, the first crack appeared approximately near the center support, i.e., 0.270 L from the center support on either side. The cracks observed were in the form of a diagonal pattern starting from the top fiber of the beam for negative moments at an average distance of 0.13 L from the center support and moving toward the bottom center of the support from both sides, as shown in Figure 16 for beam specimen 60DB3. Simultaneously, for positive moments, the cracks appeared on the bottom fiber and propagated in a diagonal pattern toward the top and end supports, as shown in Figure 17 for beam specimen 100DB2. As the load on the HPC beam increased, the cracks began to move toward the supports due to an increase in shear stress. This behavior has been observed by numerous researchers in the study of high-strength

https://doi.org/10.1021/acsomega.3c01197
ACS Omega 2023, 8, 17992−17999

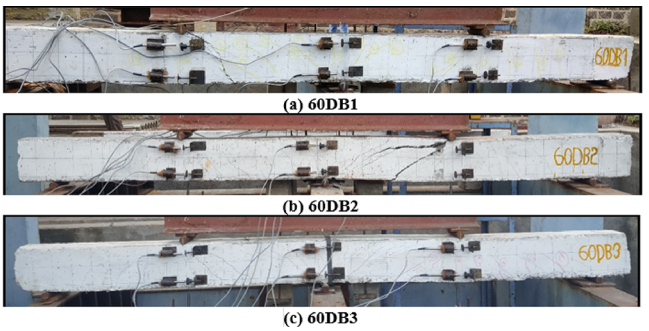

(a) 60DB1

(b) 60DB2

(c) 60DB3

Figure 13. Crack patterns and failure modes for M_{60} grade. Photograph courtesy of Aijaz Ahmad Zende. Copyright 2023.

beams, as documented in previous research papers.[28,29] However, for beam specimens 80DB1 and 80DB2, the final failure was due to shear cracks that developed at the supports. The increase in loading frequency resulted in the development of microcracks on the beams, which eventually progressed into macrocracks. In the case of specimen 60SB3, the width of the cracks at failure load reached as high as 2.6 mm. This finding is consistent with the observations made by several other researchers regarding the progression of cracks in high-strength beams under repeated loading.[30]

4.3. Crack Width. Table 4 presents the crack widths measured during the ultimate load testing of the HPC beams. The experimental results revealed that the beams displayed vertical or flexural cracks before the final failure, with cracks extending beyond the pure bending zone, like flexural cracks. The findings suggest that with an increase in concrete strength, the crack widths decrease owing to the brittle behavior of the material. However, varying the longitudinal tension reinforcement ratio had a minimal effect on crack width. Concrete strength was found to have a greater influence than longitudinal reinforcement on crack width. Longitudinal tension reinforcement can help control crack widths in HPC beams. Using mineral admixtures to produce denser concrete with a stronger interface zone can also help reduce cracks.[31]

4.4. Neutral Axis (NA) Depth Variation. Table 5 shows the NA depth variation, which was experimentally obtained by studying the strain distribution at the tension reinforcement and compression zone of concrete. The data presented in Table 5 demonstrates that there is a direct relationship between the percentage of longitudinal tension reinforcement and the depth of the neutral axis in HPC beams. As the percentage of longitudinal tension reinforcement increases, so does the depth of the NA. This is because the increase in longitudinal tension reinforcement increases the tensile capacity of the beam, which

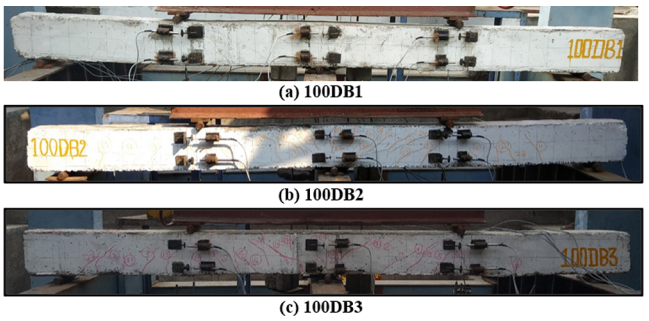

(a) 100DB1

(b) 100DB2

(c) 100DB3

Figure 15. Crack patterns and failure modes for M_{100} grade. Photograph courtesy of Aijaz Ahmad Zende. Copyright 2023.

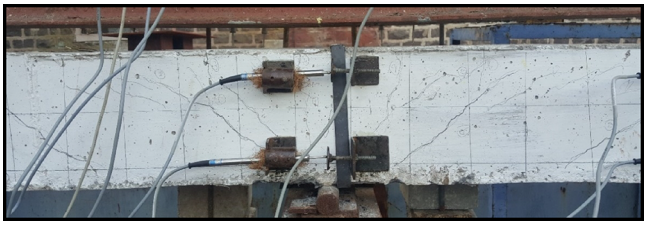

Figure 16. Crack pattern at mid-support for the M_{60} grade HPC 60DB3 beam specimen. Photograph courtesy of Aijaz Ahmad Zende. Copyright 2023.

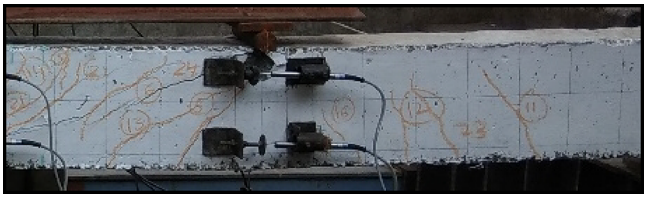

Figure 17. Crack pattern at the center of the span for the M_{100} grade HPC 100DB2 beam specimen. Photograph courtesy of Aijaz Ahmad Zende. Copyright 2023.

in turn leads to a deeper NA to resist the increased bending moment.[32] The NA depth was found to decrease just after cracking, and at a later stage, it remained the same or decreased slightly. To investigate this behavior in more detail, comparisons were made between the experimentally obtained NA depth and the predicted values from equivalent stress block parameters developed for HPC using eq 6. These comparisons are shown in Table 5. It can be observed from both results, i.e., NA depth for HPC beams obtained by experimental results and predicted using stress block parameters developed for HPC, that a lower tensile reinforcement assures a ductile failure for HPC beams for

(a) 80DB1

(b) 80DB2

Figure 14. Crack patterns and failure modes for M_{80} grade. Photograph courtesy of Aijaz Ahmad Zende. Copyright 2023.

https://doi.org/10.1021/acsomega.3c01197
ACS Omega 2023, 8, 17992−17999

Table 5. Variation of Neutral Axis Depth for Two-Span HPC Beam Specimens

beam designation	percentage of longitudinal tension steel (%)	x_{pred}/d	x_{exp}/d	$\frac{x_{exp}/d}{x_{u,max}/d}$	compressive strain at 85% of M_u	tensile strain at 85% of M_u
60DB1	1.209	0.137	0.147	0.33	0.0031	0.01805
60DB2	1.713	0.195	0.203	0.46	0.0030	0.01185
60DB3	2.173	0.251	0.257	0.58	0.0031	0.00903
80DB1	0.831	0.062	0.064	0.15	0.0031	0.04580
80DB2	0.975	0.075	0.081	0.18	0.0031	0.03519
100DB1	1.197	0.108	0.118	0.27	0.0031	0.02355
100DB2	1.713	0.154	0.162	0.37	0.0032	0.01676
100DB3	2.173	0.205	0.213	0.48	0.0033	0.01208

all the three grades of concrete (M_{60}, M_{80}, and M_{100}). It can be observed that the experimental NA depth x_{exp}/d lies between 0.147 to 0.213 and x_{pred}/d lies between 0.137 to 0.205. Thus, x_{pred}/d is in the same range of x_{exp}/d, which clarifies that the predicted stress block parameters suit the variation of NA depth for HPC. The present investigations considered an ultimate strain of 0.00375 for the development of stress block parameters to evaluate the predicted NA depth, which is higher than the ultimate strain of 0.003 mentioned by many other researchers. The ratios of $x_{exp}/d$and $x_{u,\ max}/d$ as predicted from the stress block parameters as per eq 6 are also presented in Table 5.

5. CONCLUSIONS

The present study experimentally investigated the behavior of two-span HPC beams under a monotonic five-point bending test. A total of eight beams were cast, varying the concrete grade and longitudinal tension reinforcement, to study the behavior of under-reinforced sections. The following conclusions are drawn from the present experimental work:

1. This research paper presents stress block parameters specifically for HPC. The coefficient values obtained are k_1 = 0.896, k_2 = 0.405, and k_3 = 0.77. It was found that stress block parameters designed for NSC are not suitable for HPC, and new parameters are recommended for designing HPC members.
2. The experimental results showed that increasing the percentage of longitudinal tension steel for beams of the same grade of HPC led to an increase in the load corresponding to the first visible crack. The beams failed in the tension zone, with an average of 76.70% of the ultimate load. The cracks appeared on the bottom fiber and propagated diagonally toward the top and end supports as the load increased due to an increase in shear stress.
3. Considering the experimental stress−strain curves of HPC for grades 60, 80, and 100 MPa, an idealized stress block curve is predicted using the best fitting curve. The equation for the moment of resistance of HPC beams is derived using the idealized stress block. The moment of resistance of the HPC beam specimens predicted using the derived equation agrees quite closely with the experimental flexural strength for two-span beams.
4. Based on the observation of experimental load−deformation curves, an ideal load−deformation curve is proposed, which follows four significant events identified as first cracking, yielding of reinforced steel, crushing of concrete with spalling of cover, and ultimate failure.
5. The results of the study indicate that increasing the amount of tension steel reinforcement in HPC beams can lead to a decrease in deformation capacity at a similar load level. Therefore, it is suggested that ductility can be improved by reducing the amount of tension steel reinforcement, as the longitudinal steel reinforcement ratio has a greater influence than the strength of the concrete.
6. The experimentally obtained NA depth was compared to predicted values using stress block parameters developed for HPC, and it was found that a lower tensile reinforcement assures ductile failure for HPC beams for all three grades of concrete.

AUTHOR INFORMATION

Corresponding Authors

Asif Iqbal A. Momin − *Department of Civil Engineering, BLDEA's Vachana Pitamaha Dr. P.G Halakatti College of Engineering and Technology, Vijayapur, Affiliated to VTU, Bijapur, Karnataka 586103, India*; Email: asifarzanmomin@gmail.com

Aijaz Ahmad Zende − *Department of Civil Engineering, BLDEA's Vachana Pitamaha Dr. P.G Halakatti College of Engineering and Technology, Vijayapur, Affiliated to VTU, Bijapur, Karnataka 586103, India*; Email: aijaz.52964@gmail.com

Authors

Rajesab B. Khadiranaikar − *Department of Civil Engineering, SECAB Institute of Engineering and Technology, Vijayapur, Affiliated to VTU, Bijapur, Karnataka 586109, India*

Abdullah H. Alsabhan − *Department of Civil Engineering, College of Engineering, King Saud University, Riyadh 11421, Saudi Arabia*

Shamshad Alam − *Department of Civil Engineering, College of Engineering, King Saud University, Riyadh 11421, Saudi Arabia*

Mohammad Amir Khan − *Department of Civil Engineering, Galgotia College of Engineering, Greater Noida, Uttar Pradesh 201310, India*

Mohammad Obaid Qamar − *Department of Civil Engineering (Environmental Science & Engineering), Yeungnam University, Gyeongsan 38541, South Korea*

Complete contact information is available at: https://pubs.acs.org/10.1021/acsomega.3c01197

Notes

The authors declare no competing financial interest.

ACKNOWLEDGMENTS

The authors would like to acknowledge the support provided by Researchers Supporting Project Number RSP2023R473, King Saud University, Riyadh, Saudi Arabia.

https://doi.org/10.1021/acsomega.3c01197
ACS Omega 2023, 8, 17992−17999

REFERENCES

(1) Parande, A. K. Role of ingredients for high strength and high performance concrete—a review. *Adv. Concr. Constr.* **2013 Jun**, *1*, 151.
(2) Farzadnia, N.; Ali, A. A. A.; Demirboga, R. Incorporation of mineral admixtures in sustainable high performance concrete. *Int. J. Sustain. Constr. Eng. Technol.* **2011 Jul 13**, *2* ().
(3) Cheng, B.; Gu, X.; Gao, Y.; Ma, P.; Yang, W.; Wu, J. Rheological and Mechanical Properties of High-Performance Fiber-Reinforced Cement Composites with a Low Water−Cement Ratio. *ACS Omega* **2022 Mar 9**, *7*, 9142−9151.
(4) Mehta, P. K. High-performance, high-volume fly ash concrete for sustainable development. In *Proceedings of the International workshop on sustainable development and concrete technology*; Iowa State University: Ames, IA, USA. 2004 May 14. pp. 3−14.
(5) Kodur, V. K. R.; Dwaikat, M. Flexural response of reinforced concrete beams exposed to fire. *ACI Struct. J.* **2008 Mar**, *9*, 45−54.
(6) Ahmed, G. H.; Ahmed, H.; Ali, B.; Alyousef, R. Assessment of high performance self-consolidating concrete through an experimental and analytical multi-parameter approach. *Materials.* **2021 Feb 19**, *14*, 985.
(7) Tintero, D. L.; Benito, E. K.; Maunahan, H. S.; Madlangbayan, M. S. Estimating the flexural strength of corroded reinforced concrete beams based on rectangular compressive stress block. *J. Eng. Res.* **2023 Jan 20**, *11*, No. 100005.
(8) Ng, P. L.; Barros, J. A.; Kaklauskas, G.; Lam, J. Y. K. Deformation analysis of fibre-reinforced polymer reinforced concrete beams by tension-stiffening approach. *Compos. Struct.* **2020 Feb 15**, *234*, No. 111664.
(9) Ziara, M. M.; Haldane, D.; Hood, S. Proposed changes to flexural design in BS 8110 to allow over-reinforced sections to fail in a ductile manner. *Mag. Concr. Res.* **2000 Dec**, *52*, 443−454.
(10) Ng, P. L.; Gribniak, V.; Jakubovskis, R.; Rimkus, A. Tension stiffening approach for deformation assessment of flexural reinforced concrete members under compressive axial load. *ACI Struct. J.* **2019 Dec**, *20*, 2056−2068.
(11) Wang, X.; Liu, J.; Zhang, S. Behavior of short circular tubed-reinforced-concrete columns subjected to eccentric compression. *Eng. Struct.* **2015 Dec 15**, *105*, 77−86.
(12) Gopalakrishnan, S.; Balasubramanian, K.; Krishnamoorthy, T. S.; Bharatkumar, B. H. Investigations on the flexural behavior of reinforced concrete beams containing supplementary cementitious materials. *ACI Mater. J.* **2001 Jun 1**, *199*, 645−664.
(13) Momin, A. I.; Khadirnaikar, R. B.; Zende, A. A. Flexural strength and behavioral study of high-performance concrete beams using stress-block parameters. *Int. J. Eng., Trans. B* **2021 Nov 1**, *34*, 2557−2565.
(14) Lee, C. S.; Jeon, J. S. Drift limit state predictions of rectangular reinforced concrete columns with superelastic shape memory alloy rebars. *J. Build. Eng.* **2022**, *54*, No. 104546.
(15) Kocaer, O.; Aldemir, A. Compressive stress−strain model for the estimation of the flexural capacity of reinforced geopolymer concrete members. *ACI Struct. J.*, **2022**, DOI: 10.1002/suco.202200914.
(16) Tran, T. T.; Pham, T. M.; Hao, H. Rectangular stress-block parameters for fly-ash and slag based geopolymer concrete. *InStructures*; 2019 Jun 1. *Vol. 19*. pp. 143−155 Elsevier.
(17) *State of the Art Report on High-Strength Concrete Columns. ACI 441R-1996*; American Concrete Institute.
(18) British Standard *Eurocode 2: Design of concrete structures—Part*; Thomas Telford 2004 Dec 23;*1*(1):230.
(19) *Canadian Standards Association (CSA A23.3−04). Design of concrete structures*; Canadian Standards Association: Mississauga, Ont. 2004.
(20) *Standard I. Plain and Reinforced Concrete-Code of practice (IS-456: 2000)*; Bureau of Indian Standards: New Delhi, July. 2000.
(21) Nedderman, W. H. Flexural stress distribution in very-high strength concrete. PhD diss., University of Texas at Arlington, 1973.
(22) Rusch, H. Tests on the strength of the flexural compression zone. *Bulletin Berlin, Deutscher Ausschuss Für Stahlbeton.* **1955**, *120*, 94.
(23) Ibrahim, H. H.; MacGregor, J. G. Modification of the ACI rectangular stress block for high-strength concrete. *ACI Struct. J.* **1997 Jan 1**, *94*, 40−48.
(24) Tan, T.-H.; Nguyen, N.-B. Flexural behavior of confined high-strength concrete columns. *ACI Struct. J.* **2005 Mar 1**, *102*, 198−205.
(25) Swartz, S. E.; Nikaeen, A.; Babu, H. N.; Periyakaruppan, N.; Refai, T. M. Structural bending properties of higher strength concrete. *ACI Mater. J.* **1985 Sep 1**, 147−178.
(26) Mertol, H. C.; Rizkalla, S.; Zia, P.; Mirmiran, A. Characteristics of compressive stress distribution in high-strength concrete. *ACI Struct. J.* **2008 Sep 1**, *105*, 626.
(27) Khadiranaikar, R. B.; Awati, M. M. Concrete stress distribution factors for high-performance concrete. *J. Struct. Eng.* **2012 Mar 1**, *138*, 402−415.
(28) Zende, A. A.; Khadiranaikar, R. B.; Momin, A. I. Shear Behavior of High Strength Self-Compacting Concrete Slender Beams Without Web Reinforcement. *J. Appl. Sci. Eng.* **2022 Mar**, *26*, 1.
(29) Zende, A. A.; Khadiranaikar, R. B.; Momin, A. I. A. Shear behaviour of high strength self-compacting concrete with varying stirrup spacing. *Int. J. Struct. Eng.* **2022**, *12*, 374−387.
(30) Aliş, B.; Yazici, C.; Özkal, F. M. Investigation of Fire Effects on Reinforced Concrete Members via Finite Element Analysis. *ACS Omega* **2022 Jul 20**, *7*, 26881−26893.
(31) Momin, A. I. A.; Khadiranaikar, R. B.; Zende, A. A. Modulus of Elasticity of High-Performance Concrete Beams Under Flexure-Experimental Approach. In: Ranadive, M. S.; Das, B. B.; Mehta, Y. A.; Gupta, R (eds) *Recent Trends in Construction Technology and Management. Lecture Notes in Civil Engineering*, 2023: *vol 260*. Springer: Singapore.
(32) Junaid, M. T.; Elbana, A.; Altoubat, S.; Al-Sadoon, Z. Experimental study on the effect of matrix on the flexural behavior of beams reinforced with Glass Fiber Reinforced Polymer (GFRP) bars. *Compos. Struct.* **2019 Aug 15**, No. 110930.

https://doi.org/10.1021/acsomega.3c01197
ACS Omega 2023, 8, 17992−17999